Research Article

Chitosan biopolymer based nanocomposite hydrogels for removal of methylene blue dye

Ghada A. Mahmoud[1] · Asmaa Sayed[1] · Maryan Thabit[2] · Gehan Safwat[2]

Received: 30 January 2020 / Accepted: 15 April 2020 / Published online: 25 April 2020

Abstract
Nanocomposite hydrogels were synthesized by γ-radiation-induced copolymerization and crosslinking of Chitosan biopolymer (CS), acrylic acid (AAc) and TiO_2 nanoparticles (CS-PAAc/TiO_2). The structure, morphology, and properties of the nanocomposites were investigated using Fourier-transform infrared spectroscopy, X-Ray Diffraction, Scanning electron microscopy, Transmission electron microscopy, and thermogravimetric analysis techniques. The nanocomposites hydrogel was used for the removal of methylene blue dye (MB) from wastewater. It was found that the presence of TiO_2 in the copolymeric matrix enhances the adsorption by increasing the physical interaction between the dye molecules and the adsorbent surface. The removal percentage increases with the increase in pH of the medium of all investigated samples and the maximum value is obtained at the solution pH is 10. The maximum adsorbent dosage for CS-PAAc/TiO_2 nanocomposites is 0.20 g and for CS-PAAc hydrogel is 0.15 g per liter of the adsorbate. This study revealed that the loading of TiO_2 nanoparticles into the polymeric matrix of CS-PAAc does a remarkable increase in the removal parentage of MB dye from its aqueous solution.

Keywords Gamma radiation · Nanocomposite · Chitosan · TiO_2 · Dye removal

1 Introduction

The effluent dye industry has caused severe hazards to the environment and biology due to its complex structure and chromogenic functional groups [1–3]. Among many pollutants that the mill discharges millions of gallons into the water contain naphthol, vat dyes, sulfur, nitrates, acetic acid, chromium compounds and heavy metal ions like arsenic, lead, cadmium, copper, and many other pollutants [4–6]. Most of these contaminants are hydrocarbon-based softeners, formaldehyde-based dye fixing agents and non-biodegradable dyeing chemicals [1, 2, 6]. Methylene blue dye (MB) is harm to the respiratory system and skin. It can cause vomiting and even cancer for living organisms [4]. MB absorbs light, and it affects the growth of the aquatic organisms [5]. Moreover, the aromatic structure is hardly biodegradable which means the remaining of MB for a long time if there is no adopting method for treatment [7]. Various physicochemical techniques such as adsorption, photodegradation, and membrane separation have been applied to treat the dye effluents [8]. The ideal material for efficient adsorption should possess the properties of porosity, high surface area, and physicochemical stability [9]. Bio-based adsorbents are considered one of the most promising materials in water treatment [10].

One of the most interesting materials for scientists is Chitosan (CS). It is a biodegradable, renewable, and inexpensive natural polymer [11, 12]. It has many environmentally friendly qualities and has high efficiency in water purification [13, 14]. Chitosan is used for the

✉ Asmaa Sayed, asmaasayedncrrt@gmail.com | [1]Polymer Chemistry Department, National Center for Radiation Research and Technology, Atomic Energy Authority, P.O. Box 29, Nasr City, Cairo, Egypt. [2]Faculty of Biotechnology, October University for Modern Science and Art (MSA), 6th October City, Egypt.

removal of dyes and metals [15, 16] as it has active adsorption sites like amino (-NH_2) and hydroxyl (-OH) functional groups and metals. However, it has some disadvantages for industrial applications [3], wastewater technologies, such as the too soft structure, which creates problems [17–19], its high solubility in the organic solvent, high swelling percent in water, low mechanical strength, and low surface area [20]. Many studies have been applied to improve CS properties and efficiency [21–23]. The combination of inorganic [24] and polymeric materials [25] is a successful strategy for the improvement of the restricted properties and developing new properties by introducing new functional groups that can be enhancing the ability of dye-binding [26–28]. Also improving the chemical stability of chitosan toward the acidic environment and reduce its the hydrophobicity chemical cross-linking reaction used [29]. Graft polymerization of vinyl monomers onto chitosan using gamma irradiation have been reported [30] for examples butyl acrylate onto chitosan [31], it was revealed that grafting percentage increased as the monomer concentration and the total irradiation dose were increased. Radiation grafting of acrylamide and maleic acid on chitosan and its effective application for removal of Co(II) from aqueous solutions has been studied by Saleh et al.; [32] it was found that chitosan-P(acrylamide) and chitosan-P(maleic acid) show high sorption capacity toward Co(II) as. 150 mg/g and 421 mg/g, respectively, that makes them potential sorbents of Co(II) for wastewater treatment.

In this study, (CS- PAAc/TiO_2) nanocomposite hydrogel was prepared using the gamma irradiation technique. This technique has the advantage of liberty from toxic impurities such as crosslinking agents and initiators [33, 34]. Characterization and properties the prepared nanocomposites were studied using different techniques. The influence of TiO_2 nanoparticle content on the adsorption was studied towards methyl blue dye (MB). The effect of different parameters was studied to estimate the best condition for adsorption of methyl blue dye (MB) dye that was included; pH of dye solution; adsorbent dose and temperature of the feed solution.

2 Materials and methods

Chitosan (CS) has average molecular weight 100.000–300.000 (Acros, Belgium), acrylic acid (AAc) of purity 99.9% (Aldrich) and titanium dioxide nanoparticle (TiO_2) of powder size 15 ± 3 nm (nano-gate; Egypt) were used without further purification. Other chemicals, such as buffers were purchased from El-Nasr Co. for Chemical Industries, Egypt and used without further purification.

2.1 Preparation of CS-PAAc hydrogel

CS-PAAc hydrogels were prepared by adding AAc to CS in different copolymer composition wt.%, to obtain a solution of total concentration 20 wt.%. The solution was transferred into a glass tube to be irradiated by γ-rays from Co-60 source at radiation dose of 30 kGy. The hydrogels were obtained in a long cylindrical shape and were cut into small pieces. All samples were washed in excess water to remove the unreacted component then dried in air to constant weight.

2.2 Preparation of CS-PAAc/TiO_2 nanocomposite

A solution of CS-PAAc of equal ratio was prepared as mentioned above and different content of TiO_2, 0.0, 1.0, 2.0 & 3.0 wt.% of the total polymer concentration, was added to the solution. The mixtures were sonicated in a bath sonicator for 15 min to obtain homogenous solutions. The solutions were transferred into small glass vials and were subjected to ^{60}Co-gamma rays at irradiation dose of 30 kGy. After that, the above steps of preparation CS-PAAc hydrogel were followed.

2.3 Gamma irradiation

Irradiation to the required doses was carried out in the cobalt-60 (^{60}Co) gamma cell (India) at a dose rate range from 1.77 to 2.23 kGy/min in air. This source was installed at the National Center for Radiation Research and Technology (NCRRT).

2.4 FTIR spectroscopy measurement

The infrared spectra were investigated by FTIR spectrophotometer, Spectrum One, Perkin Elmer, USA, over the range of 4000–400 cm^{-1}.

2.5 X–ray diffraction analysis (XRD)

XRD analysis was carried out using a Shimadzu Diffractometer D6000 series Kyoto, Japan. (30 mA and 40 kv) at Cu Kα (λ = 1.54 Å) radiation at room temperature in a 2θ range of 4–90 scan speed 8 deg/min. The average particle size was also calculated using the Scherer formula.

$$L_\theta = \frac{k\lambda}{\beta cos\theta} \quad (1)$$

where, L_θ is average grain size of formed crystallite and λ (1.54 Å) is the wavelength of used X-ray. β denotes the full width at half maximum (FWHM) for corresponding diffraction peak and θ is diffraction angle. k is constant (K: 0.9–1).

2.6 Scanning electron microscope (SEM)

Scanning Electron Microscope analysis (SEM) Surface of the samples was investigated by Jasco JSM-5200 scanning electron microscope (SEM), Japan with voltage accelerated at 25 kV after gold deposition in vacuum for 3 min.

2.7 Transmission electron microscopy (TEM)

The morphology of the nanocomposite was observed using transmission electron microscope (TEM) (JEOL-JEM 1400CX ELECTRON MICROSCOPE, Japan,) at acceleration voltage 80 kV. The nanocomposite sample was prepared by grinding carefully, mixed with acetone, and accompanied by a sonication process. A drop of the solution was deposited on a microgrid, to prevent the high-voltage electron beam from damaging the sample; the chamber of the sample inside the device was placed in a bath of liquid nitrogen to stabilize the temperature.

2.8 Thermal properties

Thermal Gravimetric Analysis (TGA) and differential Thermal Analysis DTA. The thermogravimetric analysis (TGA) was performed by using TGA-30 (Shimadzu, Japan) at a heating rate of 10 °C/min under the nitrogen atmosphere in the temperature range from room temperature up to 600 °C. The relative thermal stability of the samples was evaluated in terms of decomposition temperature.

2.9 Swelling properties

CS-PAAc hydrogels and CS-PAAc/TiO_2 nanocomposite hydrogels of known weights were immersed in distilled water at definite interval times until the equilibrium. The swollen samples were re-weighed after the excess surface water was removed immediately with a filter paper. The degree of swelling was determined according to the following equation:

$$Degree\ of\ Swelling\ (\%) = \frac{W_t - W_d}{W_d} \times 100 \quad (2)$$

where W_t is the weight of the sample after swelling at time t and W_d is initial of dry sample.

2.10 Point of zero charge

The pH that the charge of the adsorbent surface is zero has known as the zero point of charge (pHZPC). Zero-point charge pH of CS-PAAc/TiO_2(3.0 wt.%) was determined by the pH drift method as follows [25]:25 ml of 0.01 M NaCl solutions were poured into the beakers. The pH was adjusted 2, 4, 6, 8, 10, and 12 by adding 0.1 M HCl or 0.1 M NaOH. 0.1 g of adsorbent was then added to each beaker, and the beakers were agitated for 72 h at room temperature. Finally, the pH of solutions was measured, and the final pH was plotted against the initial pH. The zero-point charge pH is the point of intersection of the resulting curve.

2.11 Adsorption study

Batch adsorption experiments were carried out at different temperatures; 25, 35, and 50 °C. Exactly 20 ml of dye solution of known initial concentration (20 mg/L) at adjusted pH was shaken at a certain agitation speed of 250 rpm of a known dose of dried sample for 24 h.

The absorption capacity (Q_e, $mg.g^{-1}$) and MB removal percent were calculated using the following equation:

$$Q_e = \frac{(C_0 - C_e)V}{m} \quad (3)$$

$$MB\ Removal(\%) = \frac{C_0 - C_e}{C_0} \times 100 \quad (4)$$

where, C_0 and C_e (both in mg/L) are the initial dye concentration and the dye concentration at equilibrium, respectively. V is the initial solution volume (L); and m is the adsorbent dry weight (g). MB dye concentration was calculated using a UV/VIS spectrometer, model UV-Jasco V-530 made by Japan at λ_{max} of 664 nm with a quartz cell of 1.0 cm optical length.

3 Results and discussion

3.1 FTIR spectroscopy

The radiation-induced copolymerization mechanism of acrylic acid onto chitosan is shown in Scheme 1. Infrared spectroscopy analysis is an important tool to confirm the occurrence of the functional groups of the prepared hydrogel.

Figure 1 explains the FTIR spectra of CS-PAAc hydrogel and CS-PAAc/TiO_2(3.0 wt.%) nanocomposite hydrogel. For CS-PAAc hydrogel, there is broadband that

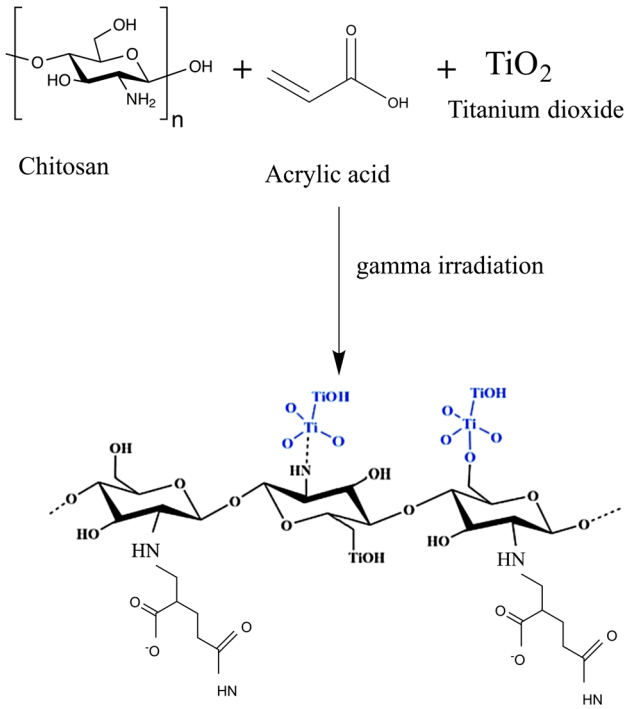

Scheme 1 Synthesis of CS-PAAc/TiO_2 nanocomposite hydrogel

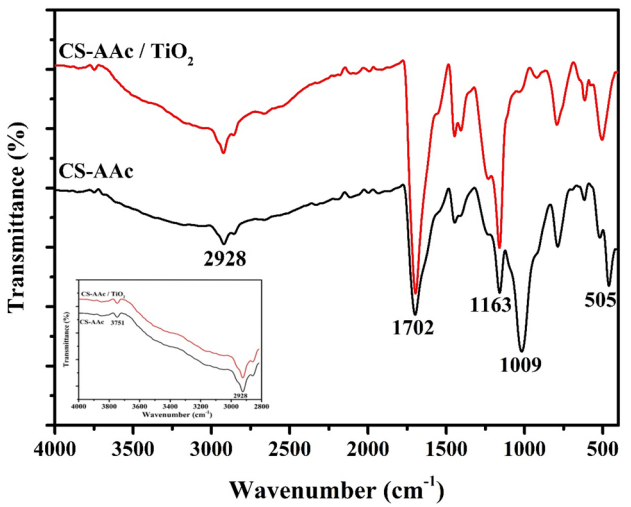

Fig. 1 FTIR spectra of CS-PAAc hydrogel and CS-PAAc/TiO_2 nanocomposite hydrogel; TiO_2 content 3.0 wt.%

appears in the range of 3678–3003 cm^{-1} due to O–H and N–H bands of AAc and CS which overlapped with the stretching band of C–H group at 2928 cm^{-1}. The band at 1702 cm^{-1} corresponds to the C = O of the carbonyl group and amide I. The band at 1590 cm^{-1} due to the N–H deformation of the amino group (amine II) [33]. For CS-PAAc/TiO_2 nanocomposite a new peak was observed at 505 cm^{-1} due to Ti–O–Ti vibration [35].

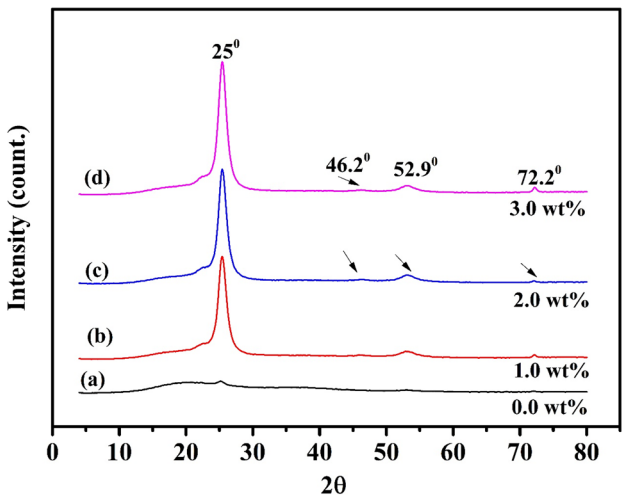

Fig. 2 XRD patterns of CS-PAAc/TiO_2 nanocomposites of different TiO_2 content

3.2 X-ray diffraction (XRD)

XRD diffractograms of CS-PAAc/TiO_2 nanocomposite hydrogels were investigated in a 2θ range of 4°–90° and the results are shown in Fig. 2. In the pattern of CS-PAAc hydrogel (0.0% TiO_2), a broad peak was observed at 2θ = 20° due to the CS-PAAc copolymer hydrogel network and confirmed the formation of an amorphous phase in the hydrogel [34]. In CS-PAAc/TiO_2 nanocomposite hydrogels patterns, sharp peaks appear at 2θ = 25° compared with the XRD pattern of the CS-PAAc hydrogel. The intensity of peaks increases as TiO_2 content increases. Moreover, the presence of low-intensity diffraction peaks at 2θ values of about 46.2°, 52.9°, and 72.2° assigned to TiO_2 nanoparticles. These diffraction peaks confirmed the presence of crystalline TiO_2 nanoparticles in the nanocomposite hydrogels [36]. The average particle size of TiO_2 nanoparticles was calculated by the Scherrer equation (Eq. 1). It is estimated as; 5.8, 5.7, and 5.9 nm for 1.0, 2.0, and 3.0 wt % TiO_2 content; respectively in the CS-PAAc/TiO_2 nanocomposite hydrogels.

3.3 Thermal properties

Thermogravimetric analysis (TGA) and differential thermal analysis (DTA) were evaluated as shown in Fig. 3. TGA determines the changes in weight as a function of temperature [37]. The TGA results [Fig. 3a] seem similar thermal behaviors and maximum thermal temperature in each stage of all investigated samples. In general, the TG curves resolved four main decomposition stages. The first decomposition stage in the range of ~ 50–180 °C due to the evaporation of the physically bonded water. This stage

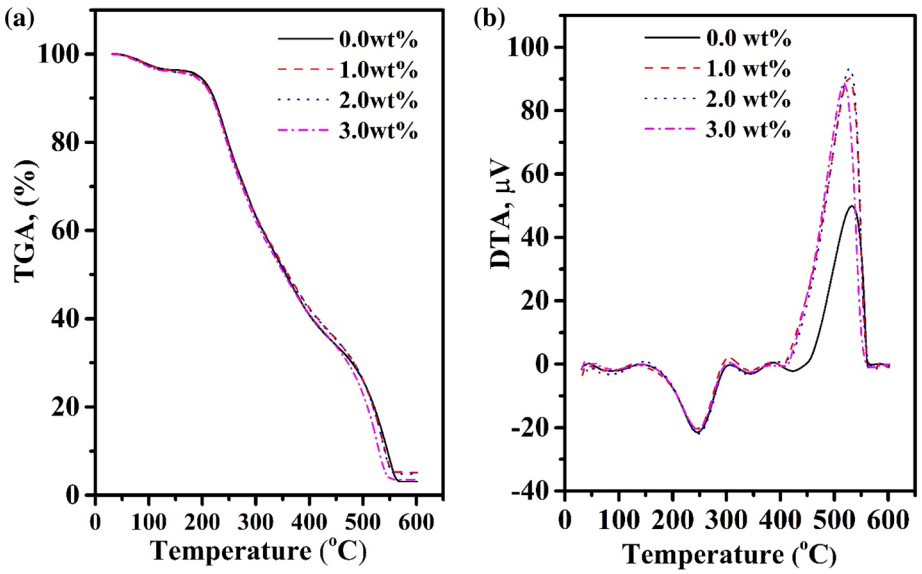

Fig. 3 **a** TGA and **b** DTA analysis of CS-PAAc hydrogel and CS-PAAc/TiO_2 nanocomposites hydrogel; TiO_2 content (0.0, 1.0, 2.0 & 3.0 wt.%)

accompanies by an endothermic peak centered at 121 °C [Fig. 3b]. The second decomposition stage in the range of 180–293 °C due to the destruction of the side groups and vaporization of voltaic compounds [38]. A broad endothermic peak centered at 253 °C accompanies this stage. The third decomposition stage occurs in the range of 293–423 °C due to due to thermal degradation of the backbone polymeric chains and accompanies by endothermic peak centered at 354 °C. The last decomposition stage was detected in the range of 423–558 °C accompanies with a sharp exothermic peak [Fig. 3b] corresponds to the transformation of the TiO_2 nanoparticles phase.

3.4 The swelling properties

The swelling of the polymeric material is important in several aspects. Water molecules may act as plasticizers relaxing interaction between the polymeric chains. Moreover, it may have a dramatic change in the permeability properties, especially in the hydrophilic polymers. Figure 4a represents the effect of CS-AAc composition on the swelling percentage. It can be seen that the swelling percentage enhances as the content of AAc is increased. It was reported that as the polymer chain backbone is built using a hydrophilic type monomer, here is (AAc), the water uptake may increase [39]. Figure 4b shows the effect of TiO_2 content on the

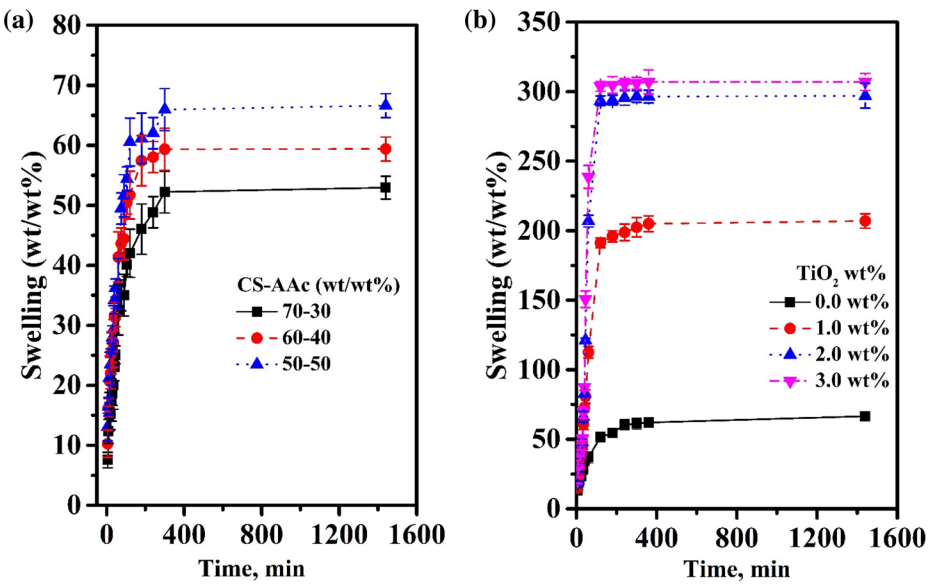

Fig. 4 **a** Effect of CS-AAc composition on the swelling percentage of CS-AAc hydrogel; **b** Effect of TiO_2 content on the swelling percentage of CS-AAc/TiO_2 nanocomposite hydrogel, CS: AAc (50:50 wt.%)

swelling percentage of CS-PAAc/TiO_2 nanocomposite hydrogels. It can be noted that the swelling percentage increases with the increase of TiO_2 content in the matrix. The swelling percentage enhances nearly fourth times by adding 1 wt.% TiO_2 nanoparticle in the nanocomposite hydrogel compared with CS-PAAc hydrogel. The increase of TiO_2 content in the nanocomposite matrix may reduce the crosslink density. Where a large free volume is available in the polymeric network consequently, more water can be absorbed [40].

3.5 Surface morphology

The surface morphology of the prepared CS-PAAc hydrogel and CS-PAAc/TiO_2 nanocomposites hydrogel was examined by SEM as shown in Fig. 5. The SEM image of CS-PAAc hydrogel [Fig. 5a] appears as a net-like structure with pores due to the hydrophilicity of both CS and PAAc, that have a great affinity to swell in water. CS-PAAc hydrogel morphology is changed drastically when loaded with TiO_2 [Fig. 5b]. The surface morphological structure of CS-PAAc/TiO_2 nanocomposite, 3 wt.% of TiO_2, appears as a compact surface with very large pores and this result illustrates the increase of the swelling percentage in the presence of TiO_2 nanoparticle.

Figure 5c shows the TEM image of CS-PAAc/TiO_2 nanocomposite hydrogel. It is clear that TiO_2 nanoparticles appears as black irregular spherical particles. The particle size is in the range of 32-59 nm. This means there is some agglomerations where the calculated particle size by the Scherrer equation is about 6 nm.

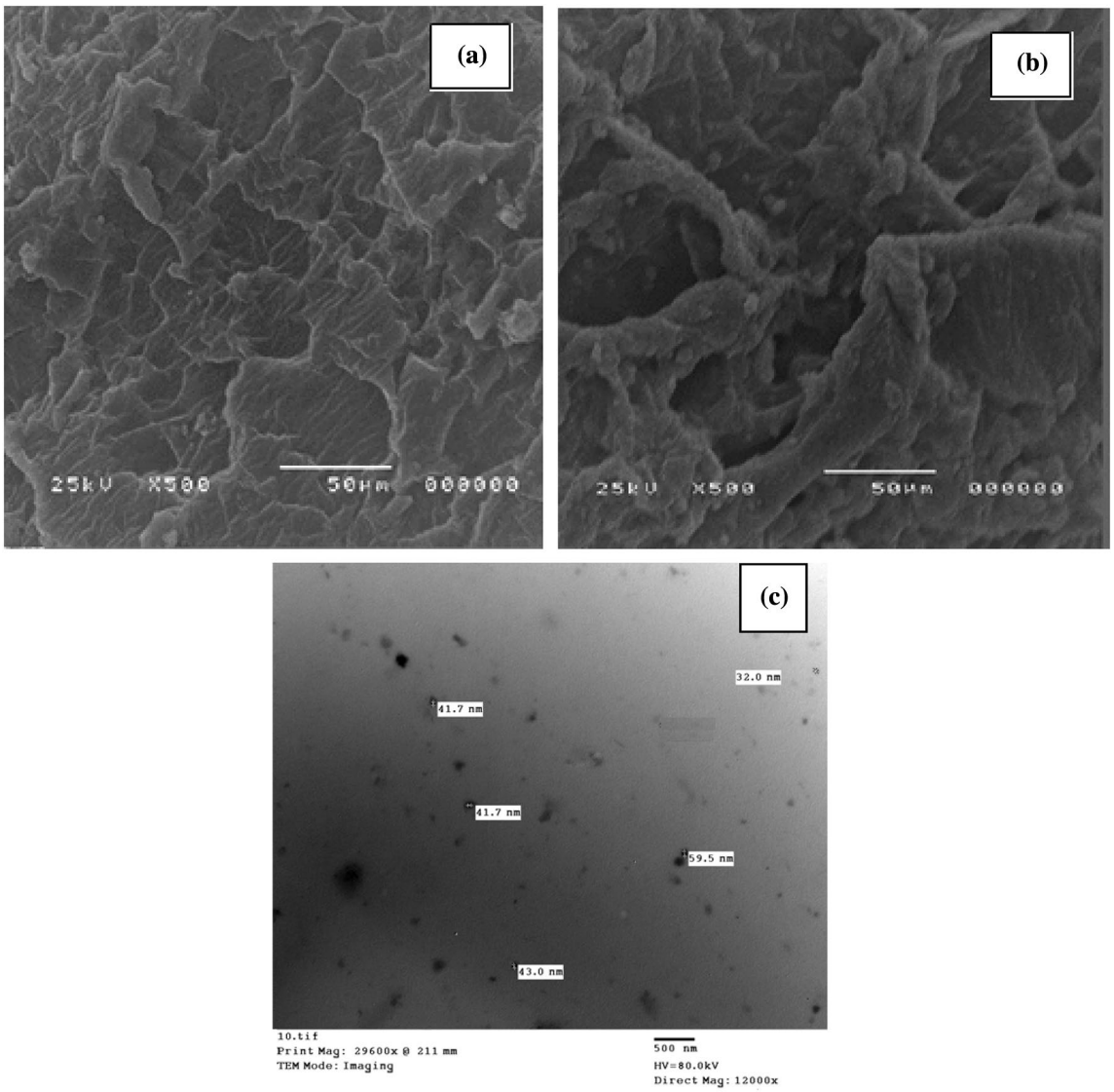

Fig. 5 **a** SEM of CS-PAAc hydrogel; **b** SEM of CS-PAAc/TiO_2 nanocompositeand **c** TEM of CS-PAAc/TiO_2 nanocomposites; TiO_2 content 3 wt.%

3.6 Adsorption study

The adsorption characteristics of the prepared CS-PAAc/TiO_2 nanocomposites towards methylene blue dye (MB) were examined. Furthermore, the adsorption behavior of CS-PAAc hydrogel (TiO_2; 0 wt.%) was also evaluated to know the influence of the presence of TiO_2 nanoparticles in the copolymeric matrix. The factors affect the adsorption behavior such as pH, adsorbent dose, and temperature were studied.

As it is clear in Fig. 6a, CS-PAAc hydrogel and CS-PAAc/TiO_2 nanocomposite hydrogel have negatively charge surface in pH range 2 to 12. It has been reported that, at pH less than pHzpc, due to the presence of the high concentration of H^+ ions in the environment, the surface charge of adsorbent is positive [41] while at pH greater than pHpzc the surface is negatively charged. The acidic character of CS-AAc/TiO_2 surface is attributted to the Acrylic acid COOH- and the acidic feature of titanium dioxide.

The influence of pH of the medium on the removal percentage of MB by CS-PAAc/TiO_2 nanocomposites was examined over pH range values between 2.0 through 10.5 and the results are shown in Fig. 6b. It was found that the removal percentage increases with the increase in pH of the medium of all investigated samples and the maximum value are got at pH 10.5. It is well known that the extent of adsorption is highly varied according to the adsorbent functional groups [42]. MB is cationic dye. At low pH values, the amino group of CS is protonated, the existence of partially positive charges on the adsorbent reduces the removal percentage by the electrostatic reparation between them and the cationic dye molecules. As the pH value increases over the pKa of –COOH which is approximately 4.6 [43] the carboxylic acid groups are ionized. An electrostatic attraction between the positively charged cationic dye and the negatively charged carboxylate anion is done which responsible for enhancing the removal percentage. On the other hand, it can be noted that CS-PAAc hydrogel (TiO_2; 0 wt) has the lowest removal percentage. An enhancement in the removal percentage was observed by using CS-PAAc/TiO_2 nanocomposites. However, no remarkable change in the adsorption was detected by increasing the TiO_2 content in the nanocomposite matrix. The presence of TiO_2 in the copolymeric matrix enhances the adsorption by increasing the physical interaction between the dye molecules and the adsorbent surface. As mentioned before in the examination of the surface morphology by SEM, the surface of the nanocomposite has very large pores compared with CS-PAAc hydrogel, Fig. 5a, b. The large pores permit the possibility of the connection between the adsorbent surface and MB molecules through the large surface area.

The influence of the adsorbent dosage on the removal percentage is shown in Fig. 7. It can be obtained that the removal percentage values increase with increasing the dosage of the sorbent from 0.05 to 0.15 g. Above this value a decrease in adsorption was observed for CS-PAAc hydrogel. In addition, a little increase in adsorption was done at 0.2 g of the two investigated nanocomposites. The maximum adsorbent dosage for the investigated CS-PAAc/TiO_2 nanocomposites is 0.20 g per liter of adsorbate and for CS-PAAc hydrogel is 0.15 g per liter

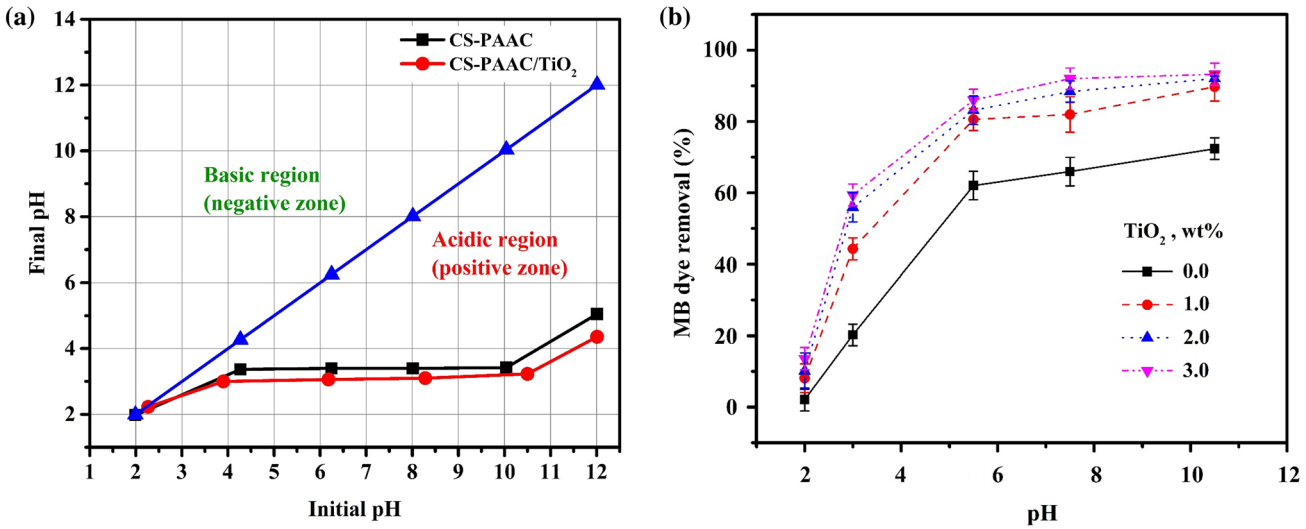

Fig. 6 **a** The pH drift method for CS-PAAc and CS-PAAc/TiO_2 nanocomposite; blue line indicates that $(pH_i) = (pH_f)$. **b** The effect of pH on the removal percentage of MB dye by CS-PAAc/TiO_2 nanocomposites at ambient temperature, initial dye concentration; 20 mg/L and contact time; 24 h

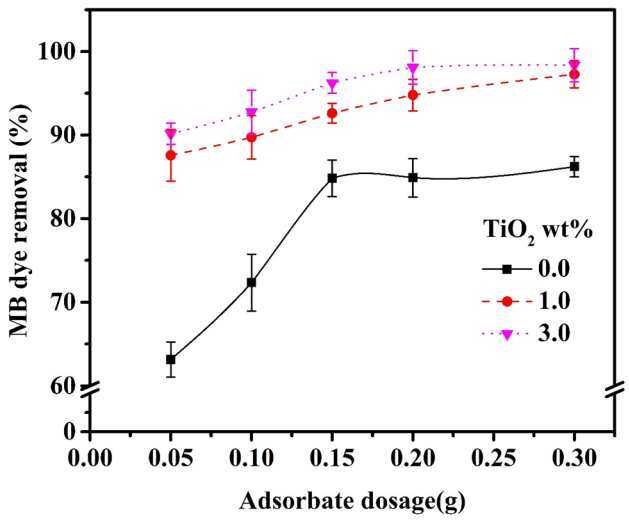

Fig. 7 The effect of the adsorbent dosage on the removal percentage of MB dye by CS-PAAc/TiO_2 nanocomposites at ambient temperature, initial dye concentration; 20 mg/L and contact time; 24 h

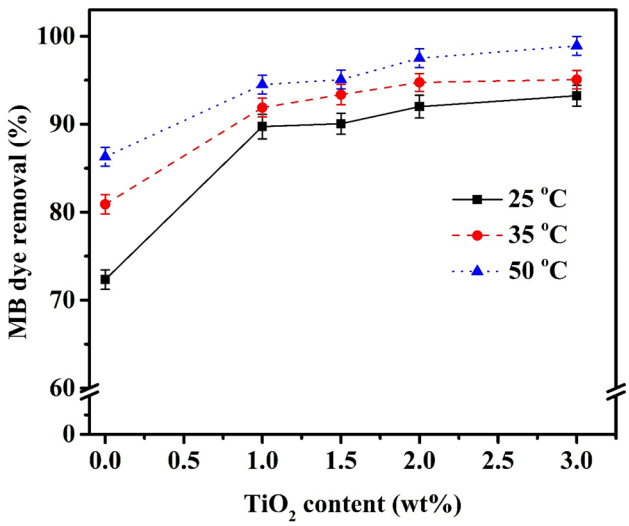

Fig. 8 The effect of TiO_2 content (wt.%) on the removal percentage of MB dye by CS-PAAc/TiO_2 nanocomposites at different temperatures, initial dye concentration; 20 mg/L and contact time; 24 h

of adsorbate. With increasing adsorbent dosage, more adsorption active sites are avaiable for adsorption of MB dye and consequently the dye removal raises. However, at higher dosage huge available functional groups on the adsorbent compared with the number of available dye molecules [44].

The influence of TiO_2 content on the removal percentage of MB dye at different temperatures is shown in Fig. 8. It can be obtained that TiO_2 does a remarkable increase in the removal parentage. The removal percentage of MB by CS-PAAc hydrogel (TiO_2; 0.0 wt.%) is 73% at 25 °C while it becomes 86% by using CS-PAAc/TiO_2 nanocomposite (TiO_2; 1.0 wt.%) at the same temperature. Above this TiO_2 content value, a little increase in the removal percentage was observed with increasing TiO_2 content in the nanocomposite.

On the other hand, an enhancement in the removal percentage was obtained by rising the temperature. This result indicated to that the adsorption reaction is endothermic.

The thermodynamics of adsorption of MB dye onto CS-PAAc and CS-PAAc/TiO_2 nanocomposite hydrogels were analyzed by the thermodynamic parameters, such as Gibb's free energy change (ΔG), enthalpy change (ΔH), and entropy change (ΔS) that can be calculated by the following equations:

$$\Delta G = -RT \ln K_C \tag{5}$$

$$K_C = \frac{Q_e}{C_e} \tag{6}$$

$$\ln K_C = \frac{\Delta S}{R} - \frac{\Delta H}{RT} \tag{7}$$

where, K_c is the thermodynamics parameter, T is the absolute temperature (K), R is the universal gas constant (8.314 J $mol^{-1}K^{-1}$). The values of ΔH and ΔS can be obtained from the slope and intercept of the linear graph about lnK_C versus 1/T, as shown in Fig. 9, respectively as listed in Table 1.

For all samples, the values of ΔG at all investigated temperatures are negative during the adsorption process. This implies that the adsorption is thermodynamically

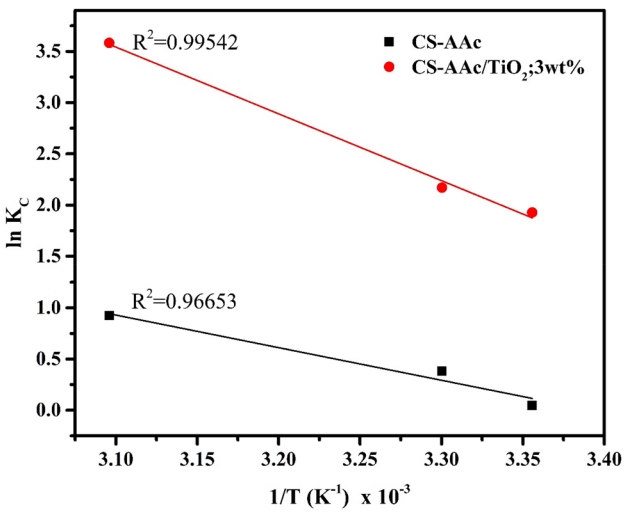

Fig. 9 Van't Hoff Plot for adsorption of MB dye onto CS-PAAc and CS-PAAc/TiO_2

Table 1 Thermodynamic parameters of MB dye removal with CS-PAAc and CS-PAAc/TiO_2

Thermodynamic parameters				
Sample	T (K)	ΔG (kJ.mol^{-1})	ΔS (kJ.mol^{-1} K^{-1})	ΔH (kJ.mol^{-1})
CS-PAAc	298	− 0.113	0.089	26.469
	308	− 0.956		
	323	− 2.480		
CS-PAAc/TiO_2; 3 wt.%	298	− 4.77567	0.198	54.193
	308	− 5.46654		
	323	− 9.62055		

favorable and spontaneous nature of the adsorption process. Moreover, the increase of the negative values of ΔG as the temperature increases indicated that the adsorption of MB onto CS-AAc and CS-AAC/TiO_2 nanocomposite hydrogel is more spontaneous at higher temperature. The positive values of ΔH confirmed the physisorption process and the endothermic nature of adsorption. ΔS also has positive values demonstrated increasing the randomness at the solid-solution interface.

4 Conclusions

In the present study, CS-PAAc/TiO_2 nanocomposite hydrogel was prepared by gamma irradiation technique. Characterization and properties were investigated. It was found that XRD diffractograms of CS-PAAc/TiO_2 nanocomposite hydrogels confirmed the presence of crystalline TiO_2 nanoparticles in the nanocomposite hydrogels. The average particle size of TiO_2 nanoparticles is estimated as; 5.8, 5.7, and 5.9 nm for 1.0, 2.0, and 3.0 wt.% TiO_2 content; respectively. The TGA results seem similar thermal behaviors and maximum thermal temperature in each stage of CS-PAAc/TiO_2 nanocomposite by varying the TiO_2content with very little change. However, the swelling percentage enhances nearly fourth times by adding 1 wt.% TiO_2 nanoparticle in the nanocomposite hydrogel compared with CS-PAAc hydrogel and there are further increases in the swelling percentage with increasing TiO_2 content in the matrix. The adsorption characteristics of the prepared CS-PAAc/TiO2 nanocomposites were studied for removal of MB dye. It was obtained that the maximum removal percentage is obtained at pH = 10.5. The maximum adsorbent dosage for CS-PAAc/TiO_2 nanocomposites is 0.20 g and for CS-PAAc hydrogel is 0.15 g per liter of the adsorbate. The removal percentage of MB by CS-PAAc/TiO_2 nanocomposite is higher than CS-PAAc hydrogel however a little increase in the removal percentage was observed with increasing TiO_2 content in the nanocomposite. The removal percentage is enhanced with rising the temperature this means the adsorption reaction is endothermic. This study revealed that the loading of TiO_2 nanoparticles into the polymeric matrix of CS-PAAc does a remarkable increase in the removal parentage of MB dye from its aqueous solution.

Compliance with ethical standards

Conflict of interest The authors declare that they have no competing interests.

References

1. Meng J et al (2019) Preparation of aminated chitosan microspheres by one-pot method and their adsorption properties for dye wastewater. R Soc Open Sci 6(5):182226
2. Turan V et al (2018) Promoting the productivity and quality of brinjal aligned with heavy metals immobilization in a wastewater irrigated heavy metal polluted soil with biochar and chitosan. Ecotoxicol Environ Saf 161:409–419
3. Sarode S et al (2019) Overview of wastewater treatment methods with special focus on biopolymer chitin-chitosan. Int J Biol Macromol 121:1086–1100
4. Chauhan M et al (2020) Investigating the efficiency of alpha-Bismuth zinc oxide heterostructure composite/UV-LED in methylene blue dye removal and evaluation of its antimicrobial activity. Environ Res 180:108857
5. Su T et al (2019) Pullulan-derived nanocomposite hydrogels for wastewater remediation: synthesis and characterization. J Colloid Interface Sci 542:253–262
6. Yu S, Wang J, Cui J (2019) Preparation of a novel chitosan-based magnetic adsorbent CTS@SnO_2@Fe_3O_4 for effective treatment of dye wastewater. Int J Biol Macromol. https://doi.org/10.1016/j.ijbiomac.2019.11.194
7. Allafchian A, Mousavi ZS, Hosseini SS (2019) Application of cress seed musilage magnetic nanocomposites for removal of methylene blue dye from water. Int J Biol Macromol 136:199–208
8. Mohammadi AA, Dehghani MH, Mesdaghinia A, Yaghmaian K, Es'haghi Z (2019) Adsorptive removal of endocrine disrupting compounds from aqueous solutions using magnetic multi-wall carbon nanotubes modified with chitosan biopolymer based on response surface methodology: functionalization, kinetics, and isotherms studies. Int J Biol Macromol. https://doi.org/10.1016/j.ijbiomac.2019.11.065
9. Wang W et al (2019) Pb(II) removal from water using porous hydrogel of chitosan-2D montmorillonite. Int J Biol Macromol 128:85–93
10. Beck BH et al (2019) Antimicrobial activity of the biopolymer chitosan against Streptococcus iniae. J Fish Dis 42(3):371–377
11. Chen S et al (2019) Core-shell biopolymer nanoparticles for co-delivery of curcumin and piperine: sequential electrostatic deposition of hyaluronic acid and chitosan shells on the zein core. ACS Appl Mater Interfaces 11(41):38103–38115
12. Wahid F et al (2017) Preparation, characterization and antibacterial applications of carboxymethyl chitosan/CuO nanocomposite hydrogels. Int J Biol Macromol 101:690–695
13. Arikal D, Kallingal A (2019) Photocatalytic degradation of azo and anthraquinone dye using TiO_2/MgO nanocomposite immobilized chitosan hydrogels. Environ Technol. https://doi.org/10.1080/09593330.2019.1701094

14. Rahman M et al (2018) Chitosan biopolymer promotes yield and stimulates accumulation of antioxidants in strawberry fruit. PLoS ONE 13(9):e0203769
15. Li C et al (2018) Fabrication of pure chitosan nanofibrous membranes as effective absorbent for dye removal. Int J Biol Macromol 106:768–774
16. Kong A et al (2018) A novel route for the removal of Cu(II) and Ni(II) ions via homogeneous adsorption by chitosan solution. J Clean Prod 192:801–808
17. Al Hosni AS, Pittman JK, Robson GD (2019) Microbial degradation of four biodegradable polymers in soil and compost demonstrating polycaprolactone as an ideal compostable plastic. Waste Manag 97:105–114
18. Franceschini G (2019) Internal surgical use of biodegradable carbohydrate polymers: warning for a conscious and proper use of oxidized regenerated cellulose. Carbohydr Polym 216:213–216
19. Hodge J, Quint C (2019) The improvement of cell infiltration in an electrospun scaffold with multiple synthetic biodegradable polymers using sacrificial PEO microparticles. J Biomed Mater Res A 107(9):1954–1964
20. Abdulhameed AS, Mohammad A-T, Jawad AH (2019) Application of response surface methodology for enhanced synthesis of chitosan tripolyphosphate/TiO_2 nanocomposite and adsorption of reactive orange 16 dye. J Clean Prod 232:43–56
21. Lima AC et al (2019) Biodegradable polymers: an update on drug delivery in bone and cartilage diseases. Expert Opin Drug Deliv 16(8):795–813
22. Lu Y et al (2019) Immobilized Candida antarctica lipase B catalyzed synthesis of biodegradable polymers for biomedical applications. Biomater Sci 7(12):4963–4983
23. Nawi MA et al (2011) Photocatalytic-oxidation of solid state chitosan by immobilized bilayer assembly of TiO_2–chitosan under a compact household fluorescent lamp irradiation. Carbohydr Polym 83(3):1146–1152
24. Nawi MA et al (2010) Adsorption of Reactive Red 4 by immobilized chitosan on glass plates: towards the design of immobilized TiO_2–chitosan synergistic photocatalyst-adsorption bilayer system. Biochem Eng J 49(3):317–325
25. Nasef SM et al (2019) Gamma radiation-induced crosslinked composite membranes based on polyvinyl alcohol/chitosan/$AgNO_3$/vitamin E for biomedical applications. Int J Biol Macromol 137:878–885
26. Maeng M et al (2019) Everolimus-eluting versus biolimus-eluting stents with biodegradable polymers in unselected patients undergoing percutaneous coronary intervention: a randomized noninferiority trial with 1-year follow-up (SORT OUT VIII Trial). JACC Cardiovasc Interv 12(7):624–633
27. Ogueri KS, Allcock HR, Laurencin CT (2019) Generational biodegradable and regenerative polyphosphazene polymers and their blends with poly (lactic-co-glycolic acid). Prog Polym Sci, 98
28. Eivazzadeh-Keihan R, Radinekiyan F, Maleki A, Salimi Bani M, Hajizadeh Z, Asgharnasl S (2019) A novel biocompatible core-shell magnetic nanocomposite based on cross-linked chitosan hydrogels for in vitro hyperthermia of cancer therapy. Int J Biol Macromol 140:407–414. https://doi.org/10.1016/j.ijbiomac.2019.08.031
29. Jawad AH, Nawi MA (2012) Oxidation of crosslinked chitosan-epichlorohydrine film and its application with TiO_2 for phenol removal. Carbohydr Polym 90(1):87–94
30. Jayakumar R et al (2005) Graft copolymerized chitosan: present status and applications. Carbohydr Polym 62(2):142–158
31. Yu L et al (2004) A new hybrid nanocomposite prepared by graft copolymerization of butyl acrylate onto chitosan in the presence of organophilic montmorillonite. Radiat Phys Chem 69(6):467–471
32. Saleh AS et al (2018) Radiation grafting of acrylamide and maleic acid on chitosan and effective application for removal of Co(II) from aqueous solutions. Radiat Phys Chem 144:116–124
33. Nasef SM, Khozemy EE, Mahmoud GA (2019) Characterization and in vitro drug release properties of chitosan/acrylamide/gold nanocomposite prepared by gamma irradiation. Int J Polym Mater Polym Biomater 68(12):723–732
34. Mohamed AA, Mahmoud GA, ElDin ME, Saad E (2019) Synthesis and properties of (Gum acacia/polyacryamide/SiO_2) magnetic hydrogel nanocomposite prepared by gamma irradiation. Polym-Plast Technol Mater. https://doi.org/10.1080/25740881.2019.1647240
35. Andreozzi M et al (2018) Treatment of saline produced water through photocatalysis using rGO-TiO_2 nanocomposites. Catal Today 315:194–204
36. Shankar S et al (2014) PII: S0268-005X (14) 00438-X
37. Martins JT et al (2012) Synergistic effects between κ-carrageenan and locust bean gum on physicochemical properties of edible films made thereof. Food Hydrocoll 29(2):280–289
38. Hegazy DE, Mahmoud GA (2014) Radiation synthesis and characterization of polyethylene oxide/chitosan-silver nanocomposite for biomedical applications. Arab J Nucl Sci Appl 47(2):1–14
39. Wojnárovits L, Földváry CM, Takács E (2010) Radiation-induced grafting of cellulose for adsorption of hazardous water pollutants: a review. Radiat Phys Chem 79(8):848–862
40. Rahim TNAT et al (2012) Water sorption characteristics of restorative dental composites immersed in acidic drinks. Dent Mater 28(6):e63–e70
41. Khairnar SD, Patil MR, Shrivastava VS (2018) Hydrothermally synthesized nanocrystalline Nb_2O_5 and its visible-light photocatalytic activity for the degradation of congo red and methylene blue. Iran J Catal 8(2):143–150
42. Mahmoud GA et al (2014) Radiation synthesis and characterization of starch-based hydrogels for removal of acid dye. Starch-Stärke 66(3–4):400–408
43. Mahmoud GA, Mohamed SF, Hassan HM (2015) Removal of methylene blue dye using biodegradable hydrogel and reusing in a secondary adsorption process. Desalin Water Treat 54(10):2765–2776
44. Khozamy E et al (2019) Implementation of carboxymethyl cellulose/acrylic acid/titanium dioxide nanocomposite hydrogel in remediation of Cd (II), Zn (II) and Pb(II) for water treatment application. Egypt J Chem 62(10):1785–1798